ARTICLE

Immunolabeling and NIR-Excited Fluorescent Imaging of HeLa Cells by Using $NaYF_4$:Yb,Er Upconversion Nanoparticles

Meng Wang,[†] Cong-Cong Mi,[†] Wen-Xing Wang,[†] Cui-Hong Liu,[†] Ying-Fan Wu,[†] Zhang-Run Xu,[†] Chuan-Bin Mao,[‡,*] and Shu-Kun Xu[†,*]

[†]College of Sciences, Northeastern University, Shenyang 110004, People's Republic of China, and [‡]Department of Chemistry & Biochemistry, University of Oklahoma, 620 Parrington Oval, Room 208, Norman, Oklahoma 73019

ABSTRACT Upconversion fluorescent nanoparticles can convert a longer wavelength radiation (*e.g.*, near-infrared light) into a shorter wavelength fluorescence (*e.g.*, visible light) and thus have emerged as a new class of fluorescent probes for biomedical imaging. Rare-earth doped β-$NaYF_4$:Yb,Er upconversion nanoparticles (UCNPs) with strong UC fluorescence were synthesized in this work by using a solvothermal approach. The UCNPs were coated with a thin layer of SiO_2 to form core—shell nanoparticles *via* a typical Stöber method, which were further modified with amino groups. After surface functionalization, the rabbit anti-CEA8 antibodies were covalently linked to the UCNPs to form the antibody—UCNP conjugates. The antibody—UCNP conjugates were used as fluorescent biolabels for the detection of carcinoembryonic antigen (CEA), a cancer biomarker expressed on the surface of HeLa cells. The successful conjugation of antibody to the UCNPs was found to lead to the specific attachment of the UCNPs onto the surface of the HeLa cells, which further resulted in the bright green UC fluorescence from the UCNP-labeled cells under 980 nm near-infrared (NIR) excitation and enabled the fluorescent imaging and detection of the HeLa cells. These results indicate that the amino-functionalized UCNPs can be used as fluorescent probes in cell immunolabeling and imaging. Because the UCNPs can be excited with a NIR light to exhibit strong visible fluorescence and the NIR light is safe to the body and can penetrate tissue as deep as several inches, our work suggests that, with proper cell-targeting or tumor-homing peptides or proteins conjugated, the $NaYF_4$:Yb,Er UCNPs can find potential applications in the *in vivo* imaging, detection, and diagnosis of cancers.

KEYWORDS: upconversion · biolabel · fluorescence · immunolabeling · cell imaging

The technique of cell immunolabeling and fluorescent imaging has been widely used in cell biology studies and clinical applications and provides a powerful tool for investigating the cellular interactions and dynamics in detail.[1] Conventional biolabels including organic dyes and fluorescent proteins have already been employed in imaging of cells and tissues. Unfortunately, they suffer from a high photobleaching rate when used in high-intensity cell imaging studies. In addition, the organic dyes are vulnerable to chemical and metabolic degradation, limiting the long-term cell tracking experiments.[2] These shortcomings have been successfully overcome by semiconductor quantum dots (QDs). QDs possess high quantum yields, bright photoluminescence, good photostability, narrow emission, and broad ultraviolet (UV) excitation, resulting in their broad applications in molecular labeling as well as cellular and *in vivo* imaging.[3−5] However, there have been wide concerns on the inherent toxicity and chemical instability of QDs.[6−8] Furthermore, the excitation of these traditional biolabels (organic dyes, fluorescent proteins, and QDs) usually requires the use of UV or short wavelength radiation, which results in a series of drawbacks: (i) low signal-to-noise ratio due to the significant autofluorescence from biological samples, (ii) low light-penetration depth inherent to the short wavelength excitation light, and (iii) possible severe cell photodamage and even the cell death caused by long-term irradiation.[9,10] Therefore, it is desirable to use fluorescent biolabels that can be excited by infrared (IR) light, and the NIR-to-visible upconversion nanoparticles (UCNPs) are a good choice. In particular, NIR light is safe to the human body and can penetrate tissue up to several inches.[11,12] Therefore, if NIR light can be used to trigger the visible fluorescence of the nanoparticles, the nanoparticles can find potential applications in *in vivo* cellular and tissue imaging.

Upconversion fluorescent nanoparticles, which can convert a longer wavelength radiation (*e.g.*, NIR light) to a shorter wavelength fluorescence (*e.g.*, visible light) *via* a two-photon or multiphoton mechanism,[13] are emerging as a new class of fluorescent biolabels. The advantages of UCNPs include their high quantum yields, narrow emis-

*Address correspondence to xushukun46@126.com, cbmao@ou.edu.

Received for review March 19, 2009 and accepted May 20, 2009.

Published online May 28, 2009. 10.1021/nn900491j CCC: $40.75

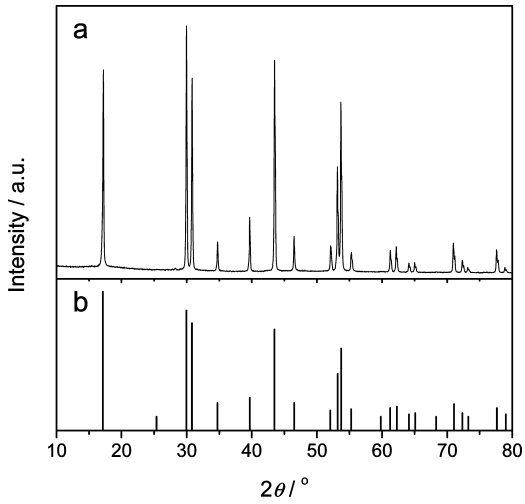

Figure 1. (a) XRD patterns of the $NaYF_4$:Yb,Er NPs; (b) calculated line pattern for hexagonal β-$NaYF_4$ (JCPDS No. 028-1192).

sion peak, large Stokes shifts, good chemical stability, and low toxicity.[14] The excitation of UCNPs often requires IR radiation, thus the signal-to-noise ratio and sensitivity of the detection can be improved due to the absence of autofluorescence.[15−17] In addition, the IR irradiation with strong penetration ability is also less harmful to cells.[18] Therefore, UCNPs are promising alternatives to traditional fluorescent biolabels for cell imaging and possess prominent potentials in biological and clinical applications.

It is well-established that hexagonal-phase (β-phase) $NaYF_4$ is one of the most efficient UC host materials under 980 nm excitation, and much attention has been paid to β-$NaYF_4$ UCNPs doped with Yb−Er or Yb−Tm rare-earth (RE) ion couples.[19−22] Up to now, β-$NaYF_4$:Yb,Er/Tm UCNPs have already been used for the detection of DNA,[23,24] avidin,[25] and the imaging of cells and tissues.[26−28] However, only limited progress has been made in biological applications, especially in immunolabeling and imaging of cancer cells. In this paper, $NaY_{0.78}F_4$:$Yb_{0.20}$,$Er_{0.02}$ UCNPs with uniform size and strong fluorescent intensity were synthesized *via* a solvothermal approach reported by us recently.[29] The as-prepared NPs were characterized by transmission electron microscopy (TEM), X-ray diffraction (XRD), Fourier transform infrared spectroscopy (FT-IR), and luminescence spectroscopy. After a typical Stöber-based surface modification, the primary amino groups were directly introduced on the surface of the UCNPs, enabling the chemical conjugation between the UCNPs and the rabbit anti-CEA8 primary antibody. Carcinoembryonic antigen (CEA), a cancer biomarker expressed on the membranes of HeLa cells, was successfully detected by fluorescence microscopic images using the antibody-conjugated $NaYF_4$:Yb,Er UCNPs. This work demonstrates that the antibody-conjugated $NaYF_4$:Yb,Er UCNPs can serve as biolabels that can specifically recognize cellular targets and exhibit very bright fluorescence for effective detection of cancer cells in biomedical applications.

RESULTS AND DISCUSSION

Synthesis and Surface Modification of $NaYF_4$:Yb,Er UCNPs. The crystal structures and the phase purity of the as-prepared $NaYF_4$:Yb,Er UCNPs were examined by XRD. Typical XRD patterns of the as-prepared UCNPs are presented in Figure 1a. The diffraction peaks of the NPs are well-defined, and the peak positions and intensities agree well with the calculated values for hexagonal β-$NaYF_4$ (line pattern in Figure 1b, JCPDS No. 028-1192), indicating that the as-prepared NPs are a highly crystalline pure hexagonal phase.

The size and morphology of the bare and surface-modified $NaYF_4$:Yb,Er NPs were characterized by TEM. Typical TEM image of the bare NPs synthesized before silica coating is shown in Figure 2a, and the NPs are well-dispersed and uniform in size with an average diameter of about 35 nm. It should be noted that the NPs synthesized even under relatively stringent conditions (for example, reacted at 150 °C for 24 h) present a regular spherical shape, which is beneficial to their further application in cellular imaging. After surface modification by SiO_2, the size of the NPs was increased to about 45 nm due to the formation of a silica layer on the surface of the bare NPs, and the shape and size monodispersity of the NPs remain almost unchanged (Figure 2b). It can be observed from Figure 2c that the thickness of the silica shell is about 5 nm.

The functional groups on the surfaces of the bare and amino-modified $NaYF_4$:Yb,Er NPs were identified

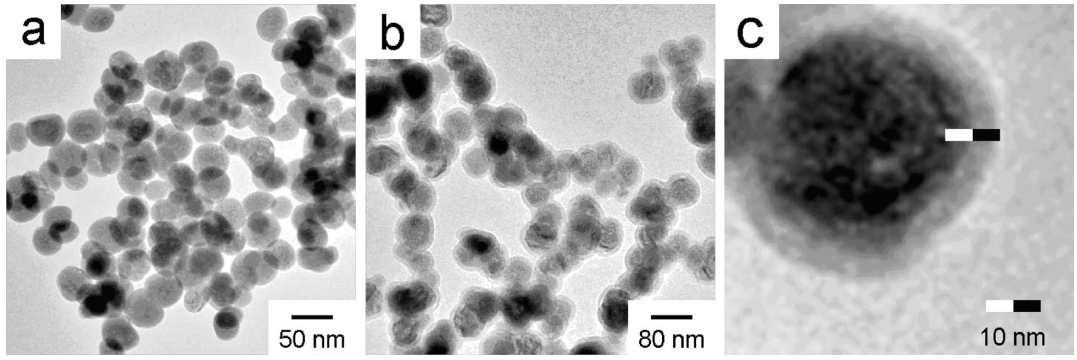

Figure 2. TEM images of bare (a) and surface-modified (b) $NaYF_4$:Yb,Er NPs. (c) Magnified version of the modified NPs.

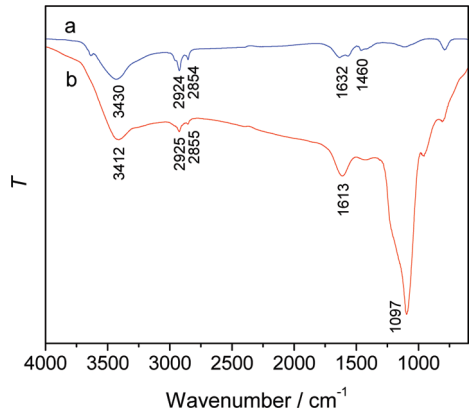

Figure 3. FT-IR spectra of bare (a) and surface-modified (b) $NaYF_4$:Yb,Er NPs.

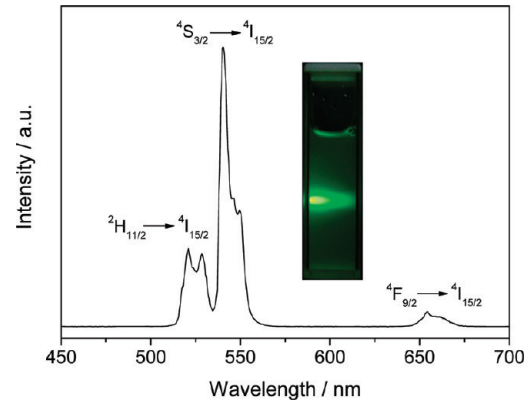

Figure 4. UC fluorescence spectra of 1 wt % colloidal solution of surface-modified $NaYF_4$:Yb,Er NPs in water. Inset is the photograph of 1 wt % colloidal solution of corresponding NPs in water, excited with a 980 nm laser.

by FT-IR spectra. The surfaces of the bare NPs are capped with a layer of oleic acid, which acts as the surfactant and capping ligands in this synthesis.[26] As shown in Figure 3a, the oleic acid exhibits a transmission band at around 3430 cm^{-1}, corresponding to the stretching vibration of hydroxyl group. Two peaks at 1632 and 1460 cm^{-1} are associated with the asymmetric and symmetric stretching vibrations of the carboxylic group (COO^-), respectively. In addition, the two peaks at 2924 and 2854 cm^{-1} can be assigned to the asymmetric and symmetric stretching vibrations of methylene group, respectively, which exists in the long alkyl chain of the oleic acid molecule. Figure 3b shows the FT-IR spectra of the amino-modified $NaYF_4$:Yb,Er NPs. The stretching and bending vibration bands of amine group appear at 3412 and 1613 cm^{-1} in the spectrum, respectively. A strong transmission band attributed to the symmetrical stretching vibration of the Si−O bond can be seen clearly at 1097 cm^{-1} in the spectrum. In addition, the two peaks at 2925 and 2855 cm^{-1} are corresponding to the asymmetric and symmetric stretching vibrations of methylene group, respectively, which exists in the hydrolysate of APTES. The peak at 1097 cm^{-1} suggests that the as-prepared NPs were successfully coated with a layer of silica, whereas the peaks at 3412, 2925, and 2855 cm^{-1} verify the binding between the functional group and shell surface.

After surface modification, the $NaYF_4$:Yb,Er NPs are stable in water and still emit strong UC fluorescence.

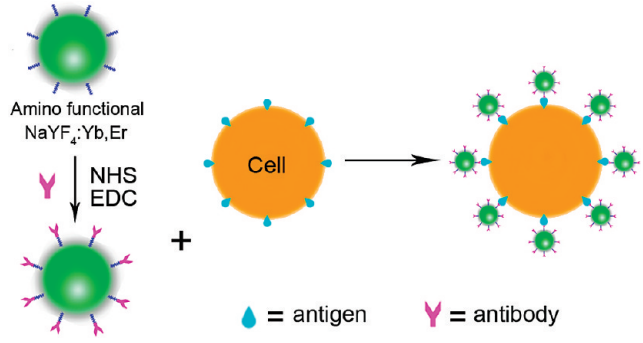

Scheme 1. Immunolabeling of HeLa cells.

The UC fluorescence properties of the surface-modified NPs were characterized by fluorescence spectra (Figure 4). The two strong green emissions at 520.5 and 540.5 nm can be assigned to the $^2H_{11/2} \rightarrow {}^4I_{15/2}$ and $^4S_{3/2} \rightarrow {}^4I_{15/2}$ transitions, respectively, whereas a weak red emission at 654.5 nm can be assigned to the $^4F_{9/2} \rightarrow {}^4I_{15/2}$ transition.[30,31] Apparently, the UC fluorescence of the colloidal solution excited with a 980 nm laser appears green in color (inset of Figure 4).

Immunolabeling and Imaging of HeLa Cells. In this work, HeLa cells were labeled by the specific recognition between the antigen expressed on the cell surface and the antibody conjugated with the UCNPs. As shown in Scheme 1, amino-modified $NaYF_4$:Yb,Er UCNPs were first cross-linked with the rabbit anti-CEA8 antibody (Ab), which involves a simple condensation reaction between carboxyl groups of antibody and amino groups on the surfaces of the NPs by the aid of NHS and EDC. After the rabbit anti-CEA8 Ab-conjugated UCNPs were incubated with BSA-blocked live cells in physiological conditions, the immunoreaction between the rabbit anti-CEA8 Ab-conjugated UCNPs and CEA8 antigens expressed on HeLa cell membrane occurred, and the UCNPs were thus linked to the surface of the cells. As a result, HeLa cells were labeled by $NaYF_4$:Yb,Er UCNPs.

To verify the immunolabeling of HeLa cells, the cells were washed after incubation with rabbit anti-CEA8 antibody−UCNP conjugates for 1 h and then imaged using a confocal microscope equipped with a 980 nm NIR laser. It can be clearly seen in Figure 5a that the cells exhibited bright green UC fluorescence, confirming the attachment of the antibody−UCNP conjugates on the surface of cells. This fact indicates that the UCNPs with good biocompatibility recognized the targets on the cell membrane due to the antibody conjugation, and the UC fluorescence was strong enough for the cell imaging. The shape and position of the cells in bright field and dark field overlapped very well, showing good specific interactions between the UCNPs and the cells. The rabbit antigoat Ab-conjugated UCNPs were incu-

bated with BSA-blocked live cells in the same physiological conditions as a negative control to verify the specific recognition and combination between the rabbit anti-CEA8 antibody-conjugated with UCNPs and the CEA8 antigens expressed on HeLa cells. Because rabbit antigoat Ab cannot be recognized specifically by the CEA8 antigen, the rabbit antigoat Ab-conjugated UCNPs could not be combined efficiently with HeLa cells, and as a result, the cells incubated with rabbit antigoat Ab-conjugated UCNPs showed very weak UC fluorescence due to the nonspecific binding, as shown in Figure 5c. The amino-modified UCNPs without linking any antibody were also incubated with BSA-blocked live cells in the same physiological conditions to investigate the nonspecific binding. As shown in Figure 5b, only little fluorescence could be observed over the surfaces of the cells due to the nonspecific binding between the UCNPs and the cells. However, the green fluorescence from nonspecific binding was very weak, which had little effect on cell imaging.

Figure 6 shows the fluorescence imaging of HeLa cells after incubated with rabbit anti-CEA8 Ab-conjugated UCNPs for different time periods. When the incubation time was 0.5 h, some weak green UC fluorescence of the UCNPs was observed from the cell membrane (Figure 6a). When the incubation time was increased to 1 h, the green UC fluorescence was enhanced (Figure 5a), indicating this immunoreaction was more complete due to extended incubation. After a longer period of incubation (*i.e.*, 6, 12, and 24 h here), the cells were still live and the strong green UC fluorescence of the UCNPs could be observed clearly from the cell membrane, suggesting that the as-prepared UCNPs are useful fluorescent probes for live cell imaging. Compared to the cells with an incubation time of 1 h (Figure 5a), the UC fluorescence intensities of the UCNPs from the cells with longer incubation time were almost unchanged, indicating that the incubation time of about 1 h is enough for this immunoreaction, and the immunolabeling method in this work was effective and time efficient.

We also studied the effect of laser power on the fluorescence imaging of the cells. As shown in Figure 7, when the excitation power of the 980 nm NIR laser was increased, the fluorescence signal from the UCNPs was also increased, which was consistent with the previous reports,[20,30] while the autofluorescence could not be observed at all. It is well-known that the cells have very low absorption of 980 nm NIR light due to the unique optical properties of the UCNPs, so the autofluorescence (noise) from cells is very low, which results in a higher signal-to-noise ratio and improved imaging of cells.[9]

Excitation of nanoparticles by NIR laser for molecular, cellular, and tissue imaging is very attractive in clinical applications because the NIR light is not harmful to the human body and can penetrate the tissue as deep

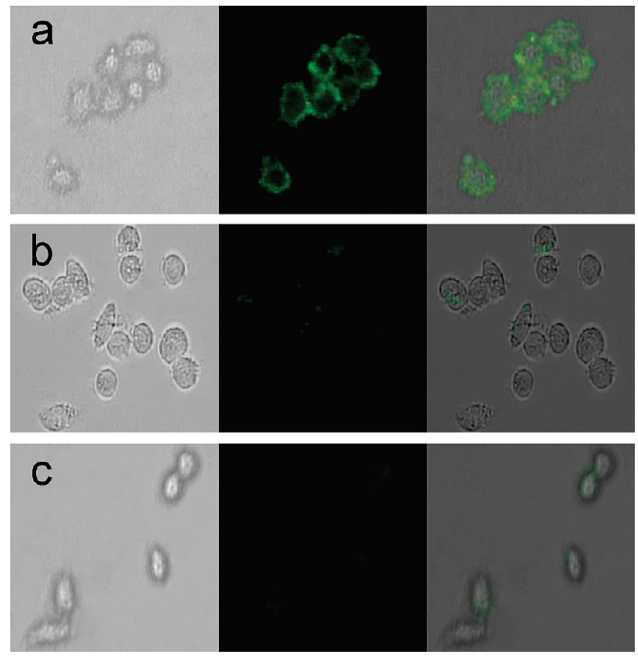

Figure 5. Fluorescence imaging of HeLa cells after incubated with rabbit anti-CEA8 Ab-conjugated UCNPs (a), amino-modified NPs without linking any antibody (b), and rabbit antigoat Ab-conjugated UCNPs (c) for 1 h. Left rows are images in bright field; the middle rows are fluorescent images in dark field; and right rows are overlays of the left and middle rows.

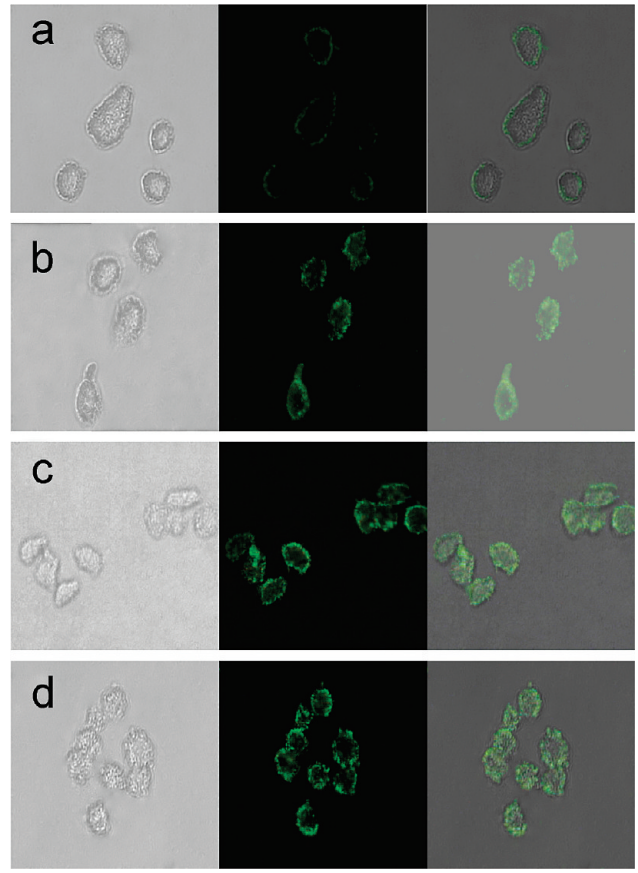

Figure 6. Fluorescence imaging of HeLa cells after incubated with rabbit anti-CEA8 Ab-conjugated UCNP conjugates for (a) 0.5, (b) 6, (c) 12, and (d) 24 h. Left rows are images in bright field; the middle rows are fluorescent images in dark field; and right rows are overlays of the left and middle rows.

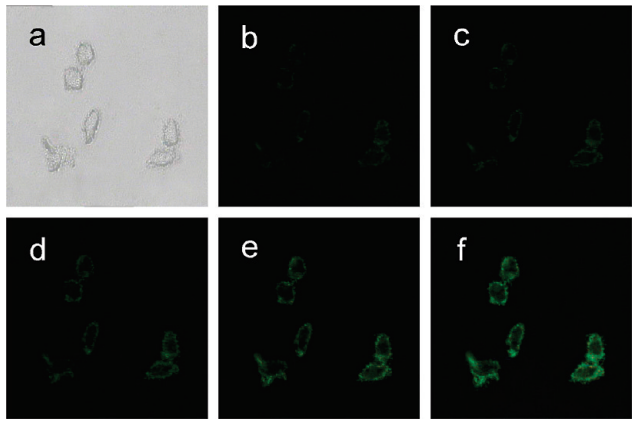

Figure 7. Fluorescence imaging of HeLa cells after incubated with rabbit anti-CEA8 Ab-conjugated UCNPs in bright field (a), and excited by a 980 nm NIR laser with different excitation powers: (b) 100, (c) 300, (d) 500, (e) 700, and (f) 900 mW.

as several inches.[11,12] Our UCNPs can be excited by NIR light and exhibit strong fluorescence. This fact suggests that our UCNPs can be applied in *in vivo* imaging. For instance, the NHS/EDC chemistry adopted in this work can be applied to conjugate our UCNPs with cancer cell-targeting or tumor-homing peptides or proteins identified by phage display technique.[32,33] The resultant conjugates can be used as fluorescent biolabels for the early detection and diagnosis of cancer. The availability of the cancer-cell targeting or tumor-homing peptides as well as the ease of conjugating them with the UCNPs will make it possible to form fluorescent probes with tunable target specificity.

CONCLUSIONS

In conclusion, amino-modified $NaYF_4$:Yb,Er UCNPs with thin and uniform silica coating on their surface were prepared. The as-prepared UCNPs were linked to the rabbit anti-CEA8 antibody to form the antibody−UCNP conjugates by a simple route, and the antibody−UCNP conjugates were used as fluorescent biolabels for the effective and time-efficient immunolabeling and imaging of HeLa cells. Strong fluorescence signal from the UCNPs was observed over the cell membrane, but no autofluorescence from the cells was found under 980 nm NIR light excitation. There was very little nonspecific binding between the UCNPs and the cells, which did not affect the cell imaging. These UCNPs are expected to be very useful for *in vitro* and *in vivo* nanomedicine studies. Further work is currently underway to use the UCNPs for *in vivo* studies.

EXPERIMENTAL SECTION

Materials. Rare-earth oxides used in this work including yttrium oxide (Y_2O_3), ytterbium oxide (Yb_2O_3), and erbium oxide (Er_2O_3) were all of 99.99% purity. Sodium fluoride (NaF), stearic acid ($C_{17}H_{35}COOH$), oleic acid ($C_{17}H_{33}COOH$), sodium hydroxide (NaOH), ammonia ($NH_3 \cdot H_2O$), nitric acid (HNO_3), and tetraethyl orthosilicate (TEOS) were of analytical grade. All the chemicals above were purchased from Sinopharm Chemical Reagent Co., Ltd. (Shanghai, China). 3-Aminopropyltrimethoxysilane (APTES, 98%), *N*-ethyl-*N*′-[3-(dimethylamino)propyl]carbodiimide hydrochloride (EDC, 98%), and *N*-hydroxysuccinimide (NHS, 98%) were purchased from Acros (USA). Primary antibody (Ab) rabbit anti-CEA8 and bovine serum albumin (BSA) were purchased from Biosynthesis Biotechnology Co. Ltd. (Beijing, China). HeLa cells were obtained from China Medical University. Triple-distilled water was used throughout the experiments.

Characterization. The size and morphology of as-prepared nanoparticles were observed on a JEM-2100HR transmission electron microscope (TEM, JEOL Ltd., Japan) using an accelerating voltage of 100 kV. XRD measurements were performed on an X'Pert Pro diffractometer (PANalytical Co., Holland) at a scanning rate of 4°/min in the 2θ range from 10 to 80°, with graphite monochromatized Cu Kα radiation (λ = 0.15406 nm). FT-IR spectra were measured on a spectrum One (B) spectrometer (Perkin-Elmer Co., USA) by the KBr method. Upconversion fluorescent spectra of the dried nanoparticles were measured on a LS-55 fluorescence spectrophotometer (Perkin-Elmer Co., USA) attached with an external 980 nm laser (Beijing Hi-Tech Optoelectronic Co., China) instead of internal excitation source. The maximum power of the laser was 1250 mW. Images in bright field and under infrared excitation were obtained using a Leica DMIL inverted fluorescence microscope equipped with a Nikon digital camera.

Synthesis of $NaYF_4$:Yb,Er UCNPs. In this synthesis, rare-earth stearate $(C_{17}H_{35}COO)_3RE$ (RE = $Y_{0.78}Y_{0.20}Er_{0.02}$) was used as a precursor.[29] A mixture of 0.8807 g of Y_2O_3, 0.3941 g of Yb_2O_3, and 0.0383 g of Er_2O_3 was dissolved in nitric acid by heating, and the solvent was evaporated to form the rare-earth nitrate powder. The as-prepared powder, 8.5344 g (30 mmol) of stearate acid, and 60 mL of ethanol were mixed in a 500 mL three-neck flask to form a transparent solution under vigorous stirring at 78 °C. Then, 1.1900 g of NaOH (30 mmol) dissolved in 15 mL of water was added dropwise into the flask, and the resultant mixture was refluxed at 78 °C for 40 min. Precipitates from the reaction mixture were filtered and washed three times with 75% ethanol. Rare-earth stearate precursor $(C_{17}H_{35}COO)_3RE$ (RE = $Y_{0.78}Y_{0.20}Er_{0.02}$) was obtained by evaporating the solvent at 60 °C for 12 h.

Subsequently, 10 mL of water, 15 mL of ethanol, and 5 mL of oleic acid were mixed together under stirring to form a homogeneous solution, to which 0.9578 g (1 mmol) of precursor and 0.2099 g (5 mmol) of NaF were added. The mixture was stirred under sonication for 15 min, transferred to a 50 mL autoclave, sealed, and solvothermally treated at 150 °C for 24 h. After the autoclave was cooled to room temperature naturally, the NPs were deposited at the bottom of the vessel, and a mixture of chloroform/ethanol (1:6, v/v) was used to collect the precipitates. The NPs were purified by centrifugation, washed with ethanol three times, and dried at 60 °C for 12 h. $NaY_{0.78}F_4$:$Yb_{0.20}$,$Er_{0.02}$ UCNPs were thus formed.

Surface Modification of $NaYF_4$:Yb,Er UCNPs. In a 250 mL flask, 20 mg of $NaYF_4$:Yb,Er UCNPs was dispersed in 60 mL of 3-propanol by sonication and agitation for 40 min. Then 2.5 mL of ammonia and 20 mL of water were added into the flask, followed by vigorous stirring at 35 °C. A solution containing 20 mL of 3-propanol and 25 μL of TEOS was added dropwise into the mixture within 1 h, and the reaction was continued for another 4 h. A solution containing 0.2 mL of APTES and 30 mL of 3-propanol was then added dropwise into the resultant mixture. After 1 h, the precipitates were separated by centrifugation, washed with ethanol three times, and dried at 60 °C for 12 h. Amino-modified $NaYF_4$:Yb,Er UCNPs were thus formed.

Conjugation of Amino-Modified UCNPs with Rabbit Anti-CEA8 Antibody. Typically, 100 μL of 0.1 mg/mL rabbit anti-CEA8 antibody (Ab) solution in 10 mmol/L phosphate buffer solution (PBS) of pH 7.4 was mixed with 100 μL of 2 mg/mL amino-modified UCNP solution in the same buffer. The mixture was activated by 50 μL of 0.2 mg/mL EDC and 25 μL of 0.2 mg/mL NHS for 10 min at room temperature, and the reaction was continued for 2 h at 37 °C in a reciprocating oscillator. The rabbit anti-CEA8 Ab-conjugated UCNPs were purified by centrifugation, washed with PBS twice, and dissolved in 2 mL of PBS. The rabbit antigoat Ab-conjugated UCNPs were prepared in the same procedure as for rabbit anti-CEA8 Ab-conjugated UCNPs except that rabbit antigoat Ab was used.

Cell Culture, Immunolabeling, and Fluorescent Imaging. The HeLa cells were cultured (at 37 °C, 5% CO_2) on glass chamber slides in RPMI 1640 medium containing 10% fetal bovine serum and 1% penicillin/streptomycin overnight in a culture box (Heraeus BB16UV). The cells were gently washed three times with PBS and blocked in PBS containing 1% bovine serum albumin (BSA) for 20 min at 4 °C. Then, HeLa cells were incubated with UCNP−antibody conjugates at 4 °C for 0.5−24 h. Prior to imaging, the live cells were washed thoroughly with PBS to remove any unbound reagents. Cell imaging was performed on a Leica DMIL inverted fluorescence microscope (with a ×40/0.5 objective) equipped with a 980 nm NIR laser and a Nikon digital camera.

Acknowledgment. We are grateful for the support from the National Science Foundation of China (Grant Nos. 20875011 and 20635010) and the Education Committee of Liaoning Province of China. C.B.M. would also like to thank U.S. National Science Foundation, Department of Defense Congressionally Directed Medical Research Program, and Oklahoma Center for the Advancement of Science and Technology for financial support.

REFERENCES AND NOTES

1. Sharma, P.; Brown, S.; Walter, G.; Santra, S.; Moudgil, B. Nanoparticles for Bioimaging. *Adv. Colloid Interface Sci.* **2006**, *123*, 471–485.
2. Lim, S. F.; Riehn, R.; Ryu, W. S.; Khanarian, N.; Tung, C. K.; Tank, D.; Austin, R. H. *In Vivo* and Scanning Electron Microscopy Imaging of Upconverting Nanophosphors in *Caenorhabditis elegans*. *Nano Lett.* **2006**, *6*, 169–174.
3. Jaiswal, J. K.; Mattoussi, H.; Mauro, J. M.; Simon, S. M. Long-Term Multiple Color Imaging of Live Cells Using Quantum Dot Bioconjugates. *Nat. Biotechnol.* **2003**, *21*, 47–51.
4. Jamieson, T.; Bakhshi, R.; Petrova, D.; Pocock, R.; Imani, M.; Seifalian, A. M. Biological Applications of Quantum Dots. *Biomaterials* **2007**, *28*, 4717–4732.
5. Bailey, R. E.; Smith, A. M.; Nie, S. M. Quantum Dots in Biology and Medicine. *Physica E* **2004**, *25*, 1–12.
6. Byrne, S. J.; Williams, Y.; Davies, A.; Corr, S. A.; Rakovich, A.; Gunko, Y. K.; Rakovich, Y. P.; Donegan, J. F.; Volkov, Y. "Jelly Dots": Synthesis and Cytotoxicity Studies of CdTe Quantum Dot-Gelatin Nanocomposites. *Small* **2007**, *3*, 1152–1156.
7. Chang, E.; Thekkek, N.; Yu, W. W.; Colvin, V. L.; Drezek, R. Evaluation of Quantum Dot Cytotoxicity Based on Intracellular Uptake. *Small* **2006**, *2*, 1412–1417.
8. Tsay, J. M.; Michalet, X. New Light on Quantum Dot Cytotoxicity. *Chem. Biol.* **2005**, *12*, 1159–1161.
9. Jalil, R. A.; Zhang, Y. Biocompatibility of Silica Coated $NaYF_4$ Upconversion Fluorescent Nanocrystals. *Biomaterials* **2008**, *29*, 4122–4128.
10. deChermont, Q. L.; Chanéac, C.; Seguin, J.; Pellé, F.; Maîtrejean, S.; Jolivet, J. P.; Gourier, D.; Bessodes, M.; Scherman, D. Nanoprobes with Near-Infrared Persistent Luminescence for *In Vivo* Imaging. *Proc. Natl. Acad. Sci. U.S.A.* **2007**, *104*, 9266–9271.
11. West, J. L.; Halas, N. J. Engineered Nanomaterials for Biophotonics Applications: Improving Sensing, Imaging, and Therapeutics. *Annu. Rev. Biomed. Eng.* **2003**, *5*, 285–292.
12. Gee, M. S.; Upadhyay, R.; Bergquist, H.; Alencar, H.; Reynolds, F.; Maricevich, M.; Weissleder, R.; Josephson, L.; Mahmood, U. Human Breast Cancer Tumor Models: Molecular Imaging of Drug Susceptibility and Dosing During HER2/Neu-Targeted Therapy. *Radiology* **2008**, *248*, 925–935.
13. Auzel, F. Upconversion and Anti-Stokes Processes with f and d Ions in Solids. *Chem. Rev.* **2004**, *104*, 139–173.
14. Wang, X.; Li, Y. D. Monodisperse Nanocrystals: General Synthesis, Assembly, and Their Applications. *Chem. Commun.* **2007**, *28*, 2901–2910.
15. Zhao, J. W.; Sun, Y. J.; Kong, X. G.; Tian, L. J.; Wang, Y.; Tu, L. P.; Zhao, J. L.; Zhang, H. Controlled Synthesis, Formation Mechanism, and Great Enhancement of Red Upconversion Luminescence of $NaYF_4$:Yb^{3+},Er^{3+} Nanocrystals/Submicroplates at Low Doping Level. *J. Phys. Chem. B* **2008**, *112*, 15666–15672.
16. Heer, S.; Kömpe, K.; Güdel, H. U.; Haase, M. Highly Efficient Multicolour Upconversion Emission in Transparent Colloids of Lanthanide-Doped $NaYF_4$ Nanocrystals. *Adv. Mater.* **2004**, *16*, 2102–2105.
17. Ehlert, O.; Thomann, R.; Darbandi, M.; Nann, T. A Four-Color Colloidal Multiplexing Nanoparticle System. *ACS Nano* **2008**, *2*, 120–124.
18. Li, Z. Q.; Zhang, Y.; Jiang, S. Multicolor Core/Shell-Structured Upconversion Fluorescent Nanoparticles. *Adv. Mater.* **2008**, *20*, 4765–4769.
19. Yi, G. S.; Chow, G. M. Synthesis of Hexagonal-Phase $NaYF_4$:Yb, Er and $NaYF_4$:Yb, Tm Nanocrystals with Efficient Up-Conversion Fluorescence. *Adv. Funct. Mater.* **2006**, *16*, 2324–2329.
20. Wei, Y.; Lu, F. Q.; Zhang, X. R.; Chen, D. P. Synthesis of Oil-Dispersible Hexagonal-Phase and Hexagonal-Shaped $NaYF_4$:Yb,Er Nanoplates. *Chem. Mater.* **2006**, *18*, 5733–5737.
21. Wang, L. Y.; Li, Y. D. Controlled Synthesis and Luminescence of Lanthanide Doped $NaYF_4$ Nanocrystals. *Chem. Mater.* **2007**, *19*, 727–734.
22. Lu, H. C.; Yi, G. S.; Zhao, S. Y.; Chen, D. P.; Guo, L. H.; Cheng, J. Synthesis and Characterization of Multi-Functional Nanoparticles Possessing Magnetic, Up-Conversion Fluorescence and Bio-Affinity Properties. *J. Mater. Chem.* **2004**, *14*, 1336–1341.
23. Wang, L. Y.; Li, Y. D. Green Upconversion Nanocrystals for DNA Detection. *Chem. Commun.* **2006**, *24*, 2557–2559.
24. Chen, Z. G.; Chen, H. L.; Hu, H.; Yu, M. X.; Li, F. Y.; Zhang, Q.; Zhou, Z. G.; Yi, T.; Huang, C. H. Versatile Synthesis Strategy for Carboxylic Acid-Functionalized Upconverting Nanophosphors as Biological Labels. *J. Am. Chem. Soc.* **2008**, *130*, 3023–3029.
25. Wang, L. Y.; Yan, R. X.; Huo, Z. Y.; Wang, L.; Zeng, J. H.; Bao, J.; Wang, X.; Peng, Q.; Li, Y. D. Fluorescence Resonant Energy Transfer Biosensor Based on Upconversion-Luminescent Nanoparticles. *Angew. Chem., Int. Ed.* **2005**, *44*, 6054–6057.
26. Chatterjee, D. K.; Rufaihah, A. J.; Zhang, Y. Upconversion Fluorescence Imaging of Cells and Small Animals Using Lanthanide Doped Nanocrystals. *Biomaterials* **2008**, *29*, 937–943.
27. Nyk, M.; Kumar, R.; Ohulchanskyy, T. Y.; Bergey, E. J.; Prasad, P. N. High Contrast *In Vitro* and *In Vivo* Photoluminescence Bioimaging Using Near Infrared to Near Infrared Up-Conversion in Tm^{3+} and Yb^{3+} Doped Fluoride Nanophosphors. *Nano Lett.* **2008**, *8*, 3834–3838.
28. Li, Z. Q.; Zhang, Y.; Jiang, S. Multicolor Core/Shell-Structured Upconversion Fluorescent Nanoparticles. *Adv. Funct. Mater.* **2008**, *20*, 4765–4769.
29. Wang, M.; Liu, J. L.; Zhang, Y. X.; Hou, W.; Wu, X. L.; Xu, S. K. Two-Phase Solvothermal Synthesis of Rare-Earth Doped $NaYF_4$ Upconversion Fluorescent Nanocrystals. *Mater. Lett.* **2009**, *63*, 325–327.
30. Boyer, J. C.; Cuccia, L. A.; Capobianco, J. A. Synthesis of Colloidal Upconverting $NaYF_4$: Er^{3+}/Yb^{3+} and Tm^{3+}/Yb^{3+} Monodisperse Nanocrystals. *Nano Lett.* **2007**, *7*, 847–852.
31. Boyer, J. C.; Vetrone, F.; Cuccia, L. A.; Capobianco, J. A. Synthesis of Colloidal Upconverting $NaYF_4$ Nanocrystals Doped with Er^{3+},Yb^{3+} and Tm^{3+},Yb^{3+} *via* Thermal

Decomposition of Lanthanide Trifluoroacetate Precursors. *J. Am. Chem. Soc.* **2006**, *128*, 7444–7445.
32. Newton, J. R.; Deutscher, S. L. *In Vivo* Bacteriophage Display for the Discovery of Novel Peptide-Based Tumor-Targeting Agents. *Methods Mol. Biol.* **2009**, *504*, 275–290.
33. Pasqualini, R.; Ruoslahti, E. Organ Targeting *In Vivo* Using Phage Display Peptide Libraries. *Nature* **1996**, *380*, 364–366.